Right- and Left-Handed Helices, What is in between? Interconversion of Helical Structures of Alternating Pyridinedicarboxamide/ m-(phenylazo)azobenzene Oligomers

Peng Tao,[†] Jon R. Parquette, and Christopher M. Hadad*

Department of Chemistry, The Ohio State University, 100 West 18th Avenue, Columbus, Ohio 43210, United States

S *Supporting Information*

ABSTRACT: Some unnatural polymers/oligomers have been designed to adopt a well-defined, compact, three-dimensional folding capability. Azobenzene units are common linkages in these oligomer designs. Two alternating pyridinedicarboxamide/m-(phenylazo)azobenzene oligomers that can fold into both right- and left-handed helices were studied computationally in order to understand their dynamical properties. Helical structures were shown to be the global minima among the many different conformations generated from the Monte Carlo simulations, and extended conformations have higher potential energies than compact ones. To understand the interconversion process between right- and left-handed helices, replica-exchange molecular dynamic (REMD) simulations were performed on both oligomers, and with this method, both right- and left-handed helices were successfully sampled during the simulations. REMD trajectories revealed twisted conformations as intermediate structures in the interconversion pathway between the two helical forms of these azobenzene oligomers. This mechanism was observed in both oligomers in current study and occurred locally in the larger oligomer. This discovery indicates that the interconversion between helical structures with different handedness goes through a compact and partially folded structure instead of globally unfold and extended structure. This is also verified by the nudged elastic band (NEB) calculations. The temperature weighted histogram analysis method (T-WHAM) was applied on the REMD results to generate contour maps of the potential of mean force (PMF). Analysis showed that right- and left-handed helices are equally sampled in these REMD simulations. In large oligomers, both right- and left-handed helices can be adopted by different parts of the molecule simultaneously. The interconversion between two helical forms can occur in the middle of the helical structure and not necessarily at the termini of the oligomer.

I. INTRODUCTION

With well-defined secondary structures, including α-helices, β-sheets, and coiled-coils, proteins possess stable tertiary structures to carry out specific biological functions. It is of great chemical and biological interest to understand the process of folding a protein's primary sequence into its secondary structure and its eventual three-dimensional (3D) shape. Besides working with natural amino acids as components of protein-based biological polymers, great efforts have been taken to design and synthesize unnatural oligomers that can fold into helical structures that resemble the natural secondary structures of proteins.[1−11] These unnatural polymers/oligomers with a well-defined, compact, three-dimensional folding capability are also termed foldamers.[12−14] The principle behind the design of these oligomers is that natural secondary structural folding driving forces, such as hydrogen bonding, Coulombic, hydrophobic, and van der Waals interactions, are universal. If designed carefully, these interactions could also drive synthetic structures being folded into well-defined structures. The folding oligomers can be divided into two categories: bioinspired and non-natural folded.[3] Most non-natural folding oligomers include aromatic rings in the backbone, thereby applying aromatic stacking effects as part of the forces for helical folding.

As with studies of protein structure, understanding the folding and the interconversion of conformational forms is essential for a rational design process of these folding oligomers. Polymers and oligomers with helical structures

have been studied for M-(minus, left-handed) and P-(plus, right-handed) helical and helical−nonhelical conformational transitions using circular dichroism and UV spectroscopy.[15−20] Several studies suggested that the helix-handedness inversion does not require a complete unfolding of a helical strand and may occur locally through the propagation of handedness changes.[21−24]
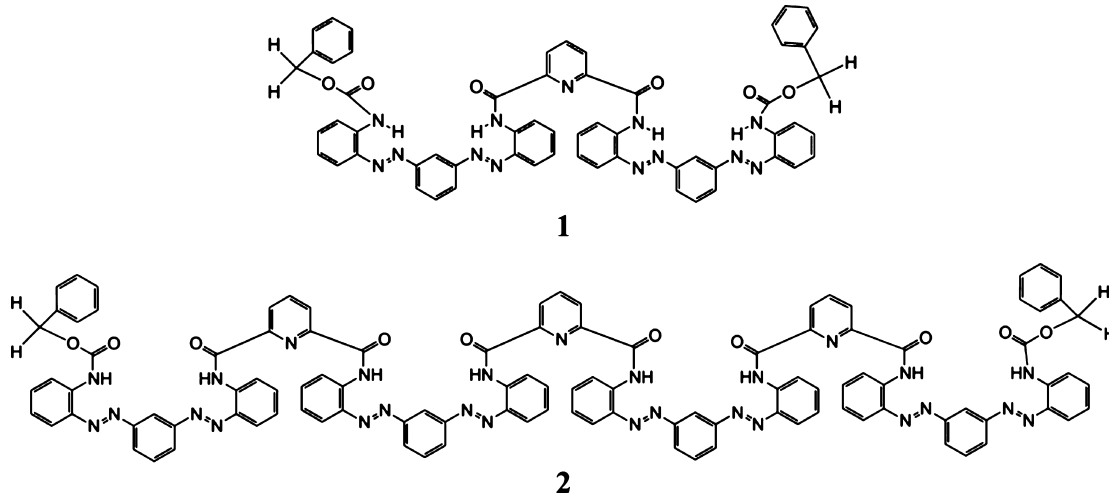
In a recent study by Parquette and co-workers,[25] alternating pyridinedicarboxamide/m-(phenylazo)azobenzene oligomers **1** and **2** were synthesized and studied (Figure 1). The crystal structure of **1** has a two-turn helical conformation with a helical pitch of approximately 3.4 Å. ^{1}H NMR spectroscopy revealed two well-separated doublets for the benzylic methylene hydrogens at the two ends of the oligomer for both **1** and **2** at low temperatures. Increasing the temperature of the NMR sample caused the two doublet peaks to gradually coalesce into a singlet for the NMR signals. At temperatures lower than the coalescence temperature, the equilibrium time scale of $M−P$ helical interconversion is slower than the NMR time scale. When above coalescence temperature, the equilibrium time scale of $M−P$ helical interconversion becomes faster than the NMR time scale, which causes the merging of two doublet

Figure 1. Alternating pyridinedicarboxamide/*m*-(phenylazo)azobenzene oligomers **1** and **2**.

peaks to one singlet NMR signal. Further evidence of the *M*−*P* chirality was obtained from subsequent simulations of the circular dichroism spectra and a comparison to experiment.[26]

Although experimental evidence suggested *M*−*P* helical structures of folding oligomers and their interconversion in these azobenzene oligomers, the mechanism of such a conversion is difficult to study experimentally because of the low barriers and the transient nature of intermediates along the interconversion pathway. Despite these difficulties, understanding the mechanism of interconversion is critical in order to optimize the folding process of non-natural helical folding oligomers. Thus, a better understanding of the molecular-level details for the interconversion process in these two oligomers, specifically the critical transition-state structures and the activation barrier for this interconversion, therefore, could lead to better design of the next generation of folding oligomers.

Computational methods can provide a complementary approach to study the preferred conformations and the interconversion processes of folding oligomers. We are particularly concerned with methods that can assist in understanding correlated motions in complex systems.[27−29] In this study, Monte Carlo (MC) conformation searches and replica-exchange molecular dynamics (REMD) methods have been applied to study the folding and interconversion between the *M* and *P* helical structures of **1** and **2**, and these results are then compared to the extant experimental results. Several single temperature MD simulations were conducted for **1**. Interconversion was not observed in any of these simulations. Because these simulations did not provide insight for the interconversion process, they are not presented in this paper.

II. COMPUTATIONAL METHODS

The systematic torsional sampling MC (SPMC)[30] search protocol implemented in Macromodel version 8.5[31] was used to sample the conformational space of **1**. A total number of 84 000 steps were performed in the MC search. The conformers generated in each step were then optimized using the AMBER* force field in water using the GB/SA solvation model.[32] All optimized conformers within 239 kcal/mol of the lowest energy were saved to ensure the coverage of both right- (*P*) and left-handed (*M*) helical structures in the conformational search. This process resulted in a total of 70 207 conformations for **1**.

Due to the complex structure of **2**, the systematic torsional protocol is not applicable for a MC conformational search. Therefore, for comparison, the MC multiple minimum (MCMM)[33,34] search protocol was used to perform a conformational search of **2**. All of the optimized conformers within 956 kcal/mol of the structure with lowest energy were saved. This process resulted in 9855 conformers of **2**.

Single point density functional theory (DFT) calculations in water using integral equation formalism polarizable continuum model (IEF-PCM)[35] for selected conformers of oligomer **1** were carried out to assess the accuracy of MC energies. Two hybrid DFT functionals, ωB97XD[36] and M06,[37] were applied for each conformer. The triple-ζ basis set 6-311++G(d,p) was shown as an appropriate choice for DFT calculations of building blocks in biomimetic systems containing aromatic rings,[38] and therefore, it was used for all the DFT calculations in present study. The ^{1}H NMR chemical shifts of the benzylic methylene hydrogens at the two ends were calculated for **1** using gauge-independent atomic orbital (GIAO) method.[39] The 6-311++G(d,p) basis set and two functionals, ωB97XD[36] and M06,[37] were used for GIAO calculations. The chemical shifts were calculated with respect to tetramethylsilane (TMS) at the same level of theory. All the DFT calculations in the study were carried out using the GAUSSIAN 09 package.[40]

Replica-exchange molecular dynamics (REMD) simulations were carried out on **1** and **2** using the AMBER8 program package.[41] The general AMBER force field (GAFF)[42] was applied to **1** and **2**. The generalized Born (GB) solvation model[43,44] was used to simulate water as a solvent. The SHAKE bond length constraints[45] were applied on all of the bonds involving hydrogen. The number of replicas of each molecule was chosen based on the size of the molecule to ensure coverage of the temperature range and exchange among replicas.[46] There were 12 replicas for **1** with temperatures set at 230.0, 245.0, 260.9, 277.8, 295.9, 315.1, 335.6, 354.0, 380.7, 405.4, 431.8, and 459.8 K. Fourteen replicas were used for **2** with temperatures set at 230.0, 241.9, 254.3, 264, 281.2, 295.7, 311.0, 327.0, 343.8, 361.6, 380.2, 399.8, 420.4, and 442.1 K. These temperatures were exponentially spaced to ensure the overlap of potential energy between two replicas with adjacent temperatures. Exchange probabilities were calculated for every 10 000 MD steps (10 ps), and there were 2200 attempts for each replica pair, resulting in 22 ns of MD simulation for each

replica. Overall, **1** had 264 ns MD simulations with 12 replicas, and **2** had 308 ns MD simulations with 14 replicas.

Starting from representative geometries from REMD simulations, transition pathways between right- and left-handed helices were searched for both **1** and **2** using the nudged elastic band (NEB) method.[47] The simulated annealing version of NEB[48] from AMBER12[49] was applied for such simulations. The initial path was heated to 300 K in 20 ps with 0.5 fs time step. Then, the path was equilibrated in 100 ps with 1 fs time step. The equilibrated path was heated to 500 K before cooling back to 300 K in 1 ns annealing simulation with 0.5 fs time step. The final path was obtained by cooling the simulated path to 0 k in 320 ps with 1 fs time step.

The temperature weighted-histogram analysis method (T-WHAM)[50] was used to combine the data of all of the replicas at different temperatures to generate the potential of mean force (PMF) of the simulated system. The WHAM method used in this study was as described by Wang and his co-workers.[51] The formalism of WHAM can be briefly reviewed as follows.[52] For a given system, the Hamiltonian $H_0(r)$ could be rewritten as a modified Hamiltonian $H_{\{\lambda\}}(r)$:

$$H_{\{\lambda\}} = H_0(r) + \sum_{i=1}^{L} \lambda_i V_i(r) = \sum_{i=0}^{L} \lambda_i V_i(r) \tag{1}$$

where $\lambda_0 = 1$ and $V_0(r) = H_0(r)$. The coordinates of the system are represented by r; $V_i(r)$ are the biasing potentials; and λ_i are the coupling parameters. For a total number of R simulations with the ith simulation performed at a temperature $\beta_i = 1/(k_B T_i)$, the probability histogram $P_{\{\lambda\},\beta}(\{V\},\xi)$ is given by

$$P_{\{\lambda\},\beta}(\{V\}, \xi) = \frac{\sum_{k=1}^{R} N_k(\{V\}, \xi)\exp(-\beta \sum_{j=0}^{L} \lambda_j V_j)}{\sum_{m=1}^{R} n_m \exp(f_m - \beta_m \sum_{j=0}^{L} \lambda_{j,m} V_j)} \tag{2}$$

with
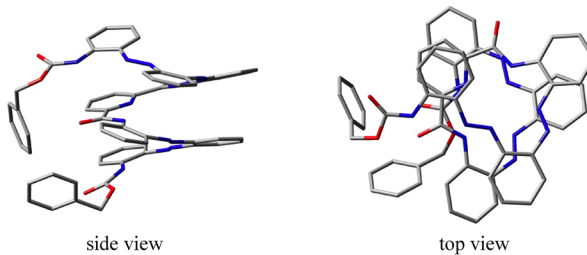
$$\exp(-f_j) = \sum_{\{V\},\xi} P_{\{\lambda\}_j,\beta_j}(\{V\}, \xi) \tag{3}$$

The $\{\lambda\}_i$ are the coupling parameters, and n_m are the number of snapshots taken. The braces $\{V\}$ denote the set of restraining potentials $V_0, V_1, ..., V_L$. In the quantity $f_j = \beta_j A_j$, A_j is the Helmholtz free energy for the jth simulation. These free energies are obtained by iterating eqs 2 and 3. The ξ corresponds to the reaction coordinate, and $N_i(\{V\},\xi)$ is the value taken by the histogram at $\{V\}$ and ξ during the ith simulation.

A principal component analysis (PCA) was carried to generate "principal" coordinates, which describe the overall conformational change of oligomers. A PCA method, called quasi-harmonic analysis, provides an efficient and well-established way to represent the conformational distribution of multidimensional systems in terms of several "principal" coordinates.[53−62] It has been shown that a large part of the system's fluctuations can be described in terms of only a few principal components.[55−59]

III. RESULTS AND DISCUSSION

A. Monte Carlo Conformational Searches of Oligomers 1 and 2.
From a MC conformational search of **1**, the conformer obtained as the global minimum is a left-handed helical structure (Figure 2). The central part of the molecule, including seven aromatic rings, forms a compact left-

Figure 2. Left-handed helical structure for the global (AMBER*) minimum of **1** (hydrogens are omitted for clarity). Side view (left) and top view (right) of the structure.

handed helix. The two benzyl rings at the ends fold back toward each other at the side of the helix. The top view of the helix reveals that two terminal benzyl rings in each ring pair are not exactly on top of each other.
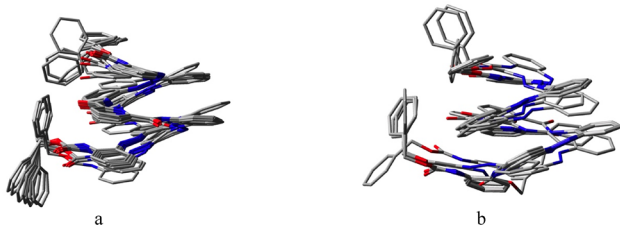
The root-mean-square deviation (rmsd) of the global minimum energy structure and the relative potential energies of the 20 lowest energy conformers are listed in Table 1. There

Table 1. 20 Most Stable Conformers of 1 Obtained from the SPMC Simulations

conformer	helical structure	potential energy (kcal/mol)[a]	rmsd (Å)		chemical shift[c]	
			I[b]	II[b]	ωB97XD[d]	M06[e]
1	left	0.0	3.1	2.0	4.81	4.66
2	left	1.8	3.2	2.0	4.84	4.69
3	right	2.0	3.4	2.0	5.13	4.95
4	left	2.1	3.5	2.0	4.91	4.91
5	left	2.1	3.4	2.1	4.79	5.02
6	right	2.2	3.7	1.9	4.70	5.19
7	left	2.2	3.5	2.0	4.89	4.83
8	right	2.2	3.4	2.0	5.07	4.89
9	left	2.2	3.5	2.1	4.77	4.84
10	left	2.3	3.4	2.1	4.80	5.00
11	left	2.3	3.5	2.0	4.89	4.89
12	left	2.4	3.5	2.1	4.70	4.74
13	right	2.5	3.4	2.0	4.69	5.10
14	right	2.5	3.6	2.0	5.11	4.80
15	left	2.5	3.1	2.0	5.01	4.85
16	right	2.6	3.5	2.0	5.05	4.78
17	left	2.7	3.5	2.1	4.79	4.71
18	right	2.7	1.8	1.5	4.15	3.99
19	left	2.8	3.9	2.0	4.70	4.60
20	left	2.9	3.5	2.0	4.93	4.68
avg.					4.84	4.81
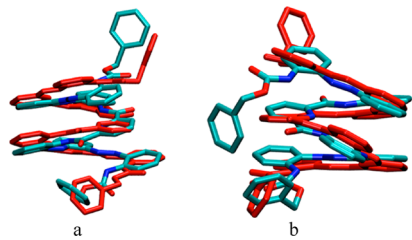
[a]Using AMBER* force field in Macromodel version 8.5. [b]rmsd I and II are for non-hydrogen atoms with reference to corresponding (right- or left-handed helix) crystal structures[25] with full structure and excluding two terminal benzyl rings, respectively. [c]Chemical shift were calculated with respect to tetramethylsilane (TMS) at the same level of theory. [d]GIAO method at IEF-PCM/ωB97XD/6-311++G(d,p) level of theory. [e]GIAO method at IEF-PCM/M06/6-311++G(d,p) level of theory.

are 13 structures among the top 20 structures, which have left-handed structures, and seven conformers with right-handed helices. These structures were superimposed on each other and shown in Figure 3; hydrogen atoms were omitted for clarity. Among these 13 left-handed conformers, four conformers have at least one terminal benzyl ring folded toward the helical

Figure 3. Overlay of the top 20 conformers of **1** as obtained from a Monte Carlo search (hydrogens are omitted for clarity). (a) Overlap of 13 left-handed helices conformers of **1**. (b) Overlap of seven right-handed helices conformers of **1**.

structure. The other nine structures with left-handed helical folds have at least one terminal benzyl ring folded away from the helical structure, in a manner that is similar to the available X-ray crystal structure of **1**.[25] These right- and left-handed structures showed similar flexibilities. Both terminal benzyl rings could point either up or down with respect to the helix. Of the 20 lowest energy structures, the seven right-handed helices are evenly distributed within the left-handed structures (Table 1). Both right- and left-handed structures are compared using their X-ray crystal structures.[25] Conformer 18 most closely resembles the crystal structure of right-handed helix with rmsd 1.8 Å of non-hydrogen atoms (Figure 4a). The major
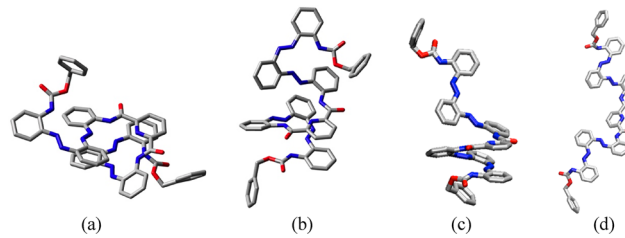
Figure 4. Superimposed crystal structures and Monte Carlo conformers: (a) crystal structure of right-handed helix of **1** (red) and conformer 18 (non-hydrogen atoms rmsd is 1.8 Å); (b) crystal structure of left-handed helix of **1** (red) and conformer 1 (non-hydrogen atoms rmsd is 3.1 Å).

difference between other helical structures and the crystal structure came from two terminal benzyl rings. When excluding two terminal benzyl rings, the non-hydrogen atoms rmsd between seven right-handed helices and crystal structure range from 1.5 to 2.0 Å (Table 1). Conformer 1 most closely resembles the crystal structure of left-handed helix with rmsd 3.1 Å of non-hydrogen atoms (Figure 4b). When excluding two terminal benzyl rings, the non-hydrogen atoms rmsd between thirteen left-handed helices and crystal structure range from 2.0 to 2.1 Å (Table 1). The ^{1}H NMR chemical shifts of the benzylic methylene hydrogens at the two ends were calculated for all 20 lowest energy conformers of **1** (Table 1). The average value was compared to the experiments. Two functionals, ωB97XD and M06, gave similar results as 4.84 and 4.81, respectively. Both are close to the experimental value (5.16).[25] The calculated chemical shifts of individual hydrogens are listed in Table S1 in the Supporting Information.

Visual inspection revealed that the higher energy structures are partially extended. One interconversion mechanism between the right- and left-handed helical structures could conveniently be proposed as a partially extended (unwound) helical structure. By partially unwinding one end of a helix, the

molecule **1** does not need to fully extend its helical structure for interconversion between the two helical forms. Conformers 5808 and 6289 display such an unwinding trend at one end of the right-handed helix (Figure 5a and b). Both conformers are

Figure 5. Conformer (a) 5808, (b) 6289, and (c) 10 000 of **1** from the Monte Carlo (AMBER*) results. (d) Extended structure of **1**.

right-handed helices; however, one end of the right-handed helix in each conformer is partially folded into a left-handed helix. If the rest of the molecule follows this trend for folding into a left-handed helix dynamically, the whole structure will convert from a right-handed to a left-handed helix. Conformers 5808 and 6289 have potential energies of 14.7 and 14.9 kcal/mol (Table 2), respectively, relative to the global minimum.

Table 2. Relative Potential Energies (kcal/mol) of Selected Conformers of 1[a]

conformer	MC[b]	ωB97XD[c]	M06[d]
1	0.0	0.0	0.0
5808	14.7	8.6	6.7
6289	14.9	6.8	4.8
10 000	27.3	16.6	14.5
extended[e]	60.4	64.9	59.5

[a]Conformer 1 is used as reference for relative potential energies. [b]Level of theory: AMBER* force field in Macromodel version 8.5. [c]Level of theory: IEF-PCM/ωB97XD/6-311++G(d,p). [d]Level of theory: IEF-PCM/M06/6-311++G(d,p). [e]A fully extended and minimized conformer of **1** (Figure 5d).
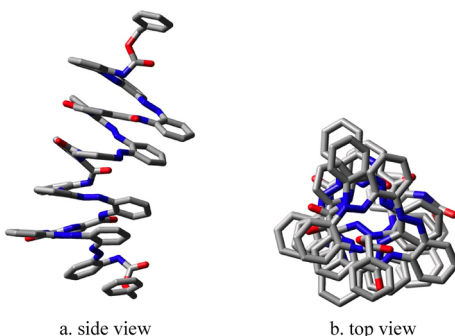
The conformer with highest energy from MC search of **1** (27.3 kcal/mol relative to the global minimum) has half of the molecule fully extended, and the other half of the molecule folded (Figure 5c). Since no fully extended conformer of **1** was observed in the MC search results, this indicates that interconversion between right- and left-handed helices can go through a half-extended conformer with a barrier that is not higher than 27.3 kcal/mol, rather than a fully extended conformer. To further validate this hypothesis, a fully extended conformer of **1** was constructed and minimized (Figure 5d) using the same level of theory in MC conformational search. The potential energy of this extended conformer is 60.3 kcal/mol higher than the global minimum. This energy gap is much higher than the highest energy gap observed in the MC conformational search.

To assess the accuracy of MC energies, the conformers 1, 5808, 6289, 10 000, and the fully extended conformer (Figure 5d) were submitted to DFT calculations. The potential energies of these conformers calculated by DFT are compared with MC results (Table 2). Two DFT functionals gave the same order of energies for chosen conformers. The order of MC energies is the same for DFT results, expect for the conformers 5808 and 6289, for which the MC energy difference is much smaller than the DFT energies. Interestingly, the relative MC energy of

extended conformer (Figure 5d) is very close to the one from DFT calculations. The difference between MC and DFT energies shows that MC mainly serves as a useful tool to explore the conformational space of target molecules. To reliably estimate the interconversion barriers in terms of free energy, the combination of REMD and T-WHAM is applied to simulate and analyze the folding process of both **1** and **2**.

The complete pathway, however, could not be identified based on the MC results, since MC simulations do not provide trajectory information. Moreover, the SPMC method allows only one variable to be randomized, and one can imagine that if coupled, or correlated, motion of one segment of the oligomers to another segment was critical. Therefore, such motion will be poorly modeled by an MC approach.
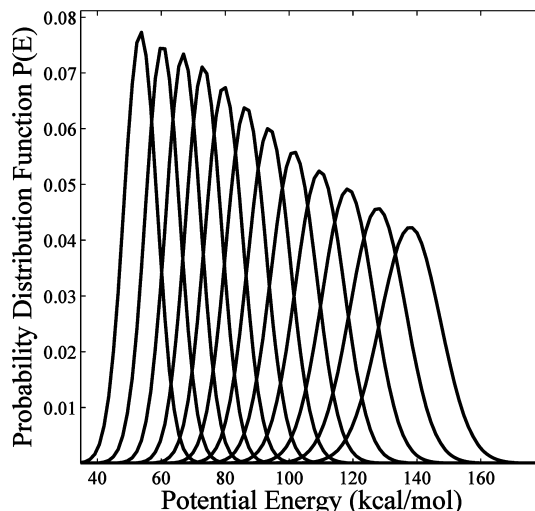
Using the MC approach, we also studied the longer oligomer **2**. The MC conformational search of **2** resulted in 9,855 unique conformers, and the lowest energy conformation has a helical structure (Figure 6). Interestingly, this helical structure is

Figure 6. Monte Carlo generated structure, with the top half being a right-handed helix and the bottom half being a left-handed helix, which has the lowest energy for **2** among other conformers (hydrogens are omitted for clarity). Side view (left) and top view (right).

neither a uniformly right-handed nor left-handed helix. Instead, the upper half (top segment in Figure 6a) has a right-handed structure, and the lower half (bottom segment in Figure 6a) has a left-handed structure. While either half of the molecule is a well-defined helix, the whole structure is well aligned along the central axis (Figure 6b). A conformer with the whole structure uniformly folded as either a right- or left-handed helix was not observed in this MC search. Careful visual investigation revealed the partially extended conformer of **2** with lowest potential energy (Supporting Information, Figure S5) is 20.2 above the minimum of MC results. There are certainly other extended conformers with higher energies. However, this observation indicates that if interconversion between different helices goes through partially extended conformers, the barrier for interconversion should not be lower than 20.2 kcal/mol. According to the NMR study, the estimated interconversion barrier for different helices of **2** is 13.8 kcal/mol.[25] Again, the difference between MC simulation and experiment suggests a nonextended interconversion mechanism of these helices.
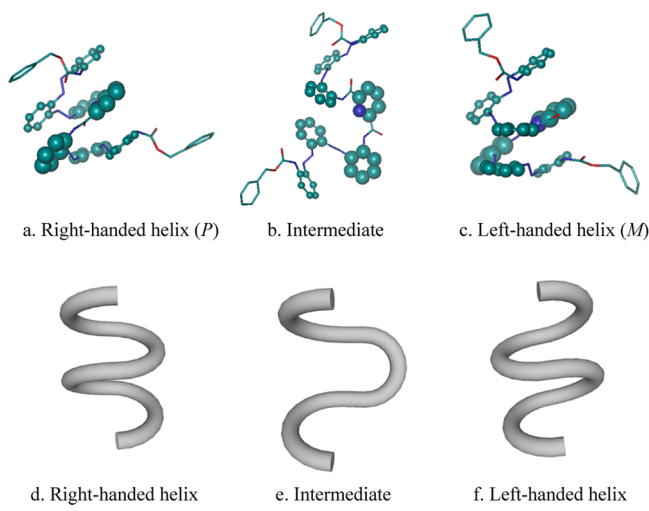
B. REMD Simulation of 1. Since single-temperature MD (300 K) simulations of both **1** and **2** did not show any interconversion between the two helical forms (see the Supporting Information), replica exchange molecular dynamics (REMD) methods were applied to simulate the interconversion of **1** with 12 replicas at different temperatures. The potential energy histograms of these 12 replicas of **1** at each target temperature are shown in Figure 7. The potential energy

Figure 7. Potential energy histograms of 12 replicas in the REMD simulation of **1**.

distribution of each replica significantly overlaps with each other, ensuring a high exchange rate. The average acceptation ratio for exchange is 0.490 for REMD simulation of **1**. The acceptation ratio for each individual replica is listed in Table S2 in the Supporting Information. The Boltzmann distribution of the potential energy of each replica also indicates that equilibrium was achieved in this series of simulations.
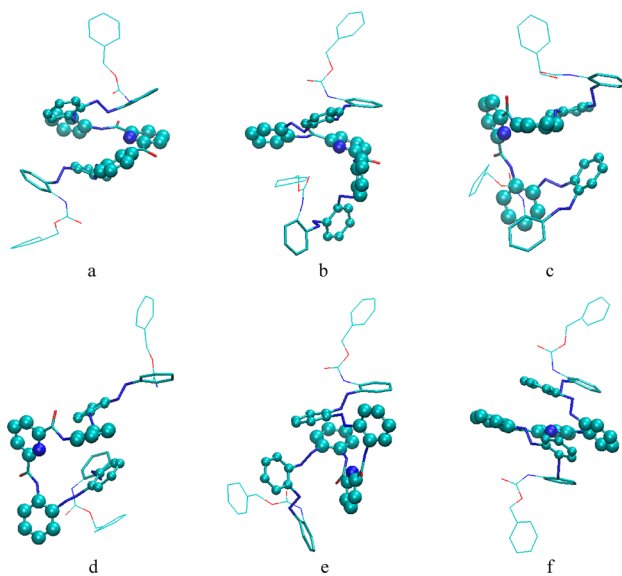
After careful tracing of trajectories through different replicas, the "mechanism" of interconversion between helical structures of **1** was mapped, and these structures are illustrated in Figure 8. In this mechanism, **1** does not go through an extended conformation in order to interconvert between helices. Instead, a compact intermediate structure was observed as connecting helices (Figure 8b). The conversion of a helix is mainly involved with orientation of the two aromatic rings (Figure 8a–c, two highlighted rings). Originally, these two rings have the same orientation as the rest of the molecule in a right-handed

a. Right-handed helix (*P*)   b. Intermediate   c. Left-handed helix (*M*)

d. Right-handed helix   e. Intermediate   f. Left-handed helix

Figure 8. Mechanism of interconversion between the two helical forms of **1** (hydrogens are omitted for clarity). Top row actually contains structures of **1** from the folding path. Bottom row is the cartoon illustration of the folding path. See text for a discussion of the interconversion process and the Supporting Information for a movie clip.

helix (Figure 8a, two highlighted rings). During the conversion process, these two rings, and the pyridinedicarboxamide linkage between them, rotate counterclockwise to reach the intermediate structure (Figure 8b), but no significant changes occur in the *syn*−*syn* preference[63] of the pyridinedicarboxamide linkage during this conversion. The intermediate structure is still compact, but the helical structure of the central part is unwound. Those two rings then keep rotating counterclockwise; the left-handed helix is thus formed, and the interconversion is completed (Figure 8c). During this process, the motions of the two terminal benzyl rings are coupled with the conformational change of the central part. Along with the helical interconversion of the central part of **1**, the orientations of the two terminal benzyl rings changed simultaneously from right- to left-handed. The cartoon in the bottom row of Figure 8 illustrates this process.

To further illustrate this mechanism, several representative snapshots from a continuous trajectory identified in REMD simulations representing transition between two helices are shown in Figure 9. It is clearly shown that, in the conversion from a right-handed helix (Figure 9a) to a left-handed helix (Figure 9f), oligomer **1** went through a series of compact intermediate structures (in contrast to a fully extended structure), which are mainly involved with rearrangements of the central five six-membered rings. A short movie illustrating this transformation (Figure 9c−f) is also available in the
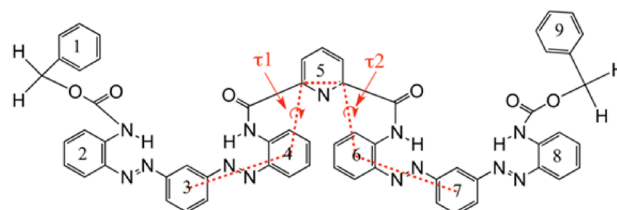
Figure 9. Snapshots along the interconversion pathway between the *M* and *P* configurations of **1** from REMD trajectories. (a) *P* configuration (right-handed helix) of **1**. (b) Bottom half of **1** is twisted. (c) **1** is transformed into a twisted intermediate structure. (d) Rearrangement of twisted intermediate structure of **1**. (e) Twisted intermediate structure of **1** changes to a more compact form before folding to left-handed helix. (f) *M* configuration (left-handed helix) of **1**. Atoms are colored according to atom types (C, N, and O are shown in cyan, blue, red, respectively). Hydrogen atoms are not shown for clarity. Different parts of the molecule are shown in different forms for easier viewing: the two terminal benzyl rings and carboxamide linkers are shown in line format; the two benzyl rings next to the terminal benzyl rings and all other linkages are shown in tube format; five central six-membered rings are shown in ball-and-stick format. A short molecular dynamics movie showing conformational change from twisted intermediate structure to left-handed helix is provided in the Supporting Information.

Supporting Information. The observed helical structures of REMD are compared with crystal structures of **1** (see the Supporting Information, Figure S6).[25] Non-hydrogen atom RMSDs of right- and left-handed helices with reference to corresponding crystal structures are 4.2 and 3.8 Å, respectively. When excluding two terminal benzyl rings, the RMSDs for right- and left-handed helices are 2.7 and 2.8 Å, respectively. Because the structures from REMD simulations are generally away from energy minima, these numbers are higher than rmsd between MC conformers and crystal structures.

C. NEB Reaction Path for Helical Interconversion of 1. The geometries shown in Figure 9 were used to construct the initial path for NEB calculations of **1**. A total of 16 replicas were built for the NEB path by making multiple copies for initial geometries. The final path demonstrates that the interconversion between two helices could be achieved through the local movement of structure (Figure S7 in the Supporting Information).
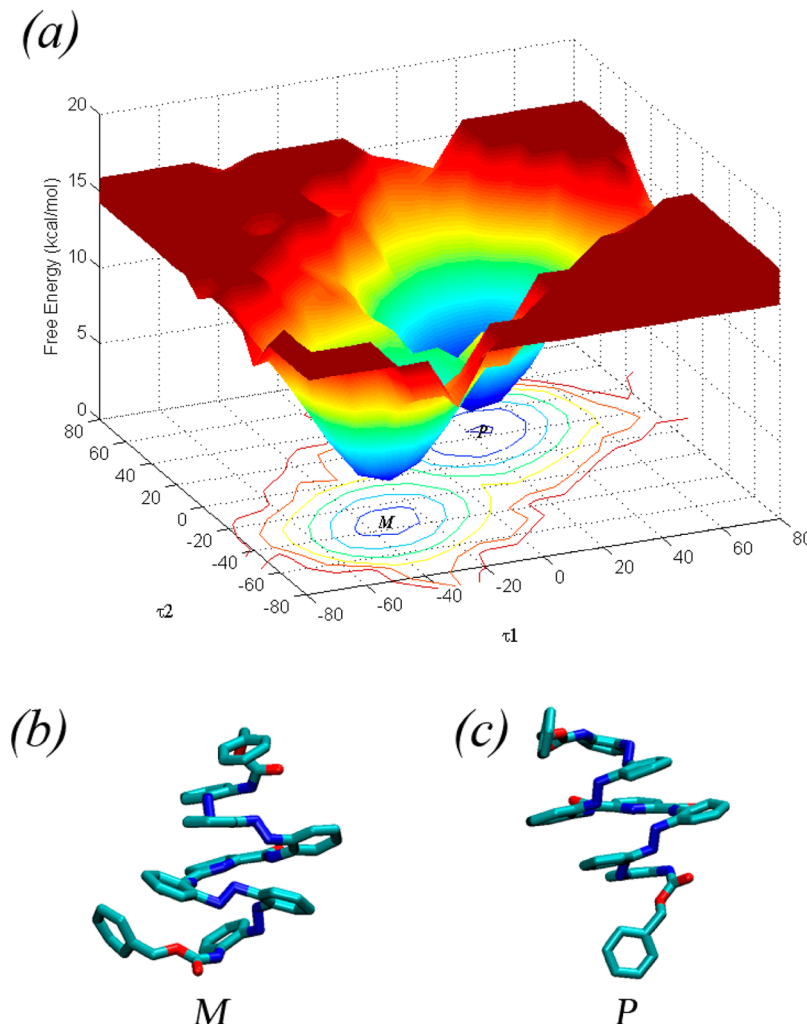
D. Potential of Mean Force of 1. In helical structures, the position and orientation of the central pyridinedicarboxamide unit and the azobenzene rings are correlated to each other. Two dihedral angles (τ_1 and τ_2), which are highly correlated to the helical conformations, are defined in Figure 10. The

Figure 10. Definitions of dihedral angles (τ_1 and τ_2) of **1** for WHAM analysis. The two dihedral angles are defined by two carbon atoms adjacent to the nitrogen in the central pyridine ring (ring 5) and the centroids of two benzene rings next to pyridine on either side (ring 3, 4, 6, and 7).

distribution of these dihedral angles reflects the distribution in conformational space of **1**. These two dihedral angles were chosen for T-WHAM analysis to generate a potential of mean force (PMF) for **1**.

The PMF of the Gibbs free energy at 300 K projected onto dihedral angles 1 (τ_1) and 2 (τ_2) are shown in Figure 11a. There are two basins of attraction located on the diagonal line. One basin is centered at the combination of both τ_1 and τ_2 with values around −40°. This region is associated with an *M* configuration (left-handed helix) of **1** (Figure 11b). The other one is centered at the combination of two angles with values around 40°. This region is associated with a *P* configuration (right-handed helix) of **1** (Figure 11c). This potential energy surface shows that the two helical structures are the two global minima of **1**. Both helices are energetically equivalent in the simulation. There is no other attraction basin shown in this surface, and the two attraction basins with low free energies are symmetric with respect to the origin, $\tau_1 = \tau_2 = 0$ and the diagonal, $\tau_1 = \tau_2$. This symmetry reflects the fact that the *M* and *P* configurations of **1** are mirror images of each other and provides further confidence in the statistical sampling of these REMD trajectories. The interconversion barrier between two helices of **1** is approximately 10 kcal/mol according to the potential energy surface shown in Figure 10a. This is in very
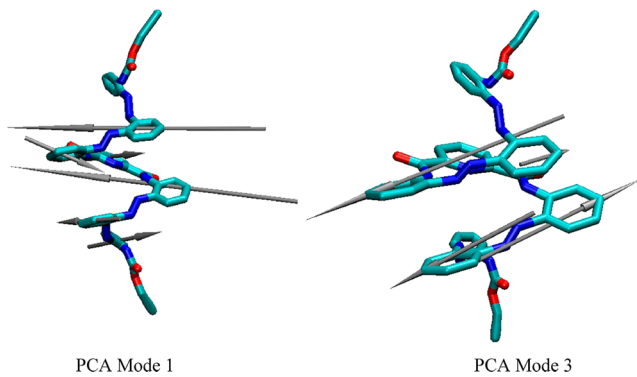
Figure 11. Potential of mean force (PMF) from the REMD simulation of **1**. (a) The contour plots of the Gibbs free energy (G) at 300 K projected onto the dihedral angle τ_1 and dihedral angle τ_2 as "reaction coordinates" in **1** (see Figure 9). (b) *M* configuration (left-handed helix) of **1**. (c) *P* configuration (right-handed helix) of **1**. The reaction barrier for interconversion between *M* and *P* configurations of **1** is ~10 kcal/mol according to the PMF shown in (a).

good agreement with the experimental value of 11.1 kcal/mol as determined by variable temperature NMR.[25]

The allowance range of each dihedral angle is approximately ±80°, as shown in the PMF surface of **1**. This indicates that these two angles are strongly coupled to each other and cannot arbitrarily reach any value as a combination. The most probable pathway for a molecule converting between the *M* and *P* regions is following the straight line directly through the origin, and at the origin, both dihedral angles have values of zero. This seems energetically unfavorable upon initial chemical intuition. However, the PMF plot does not show this region as unreachable for the molecule, but quite well populated compared to other regions adjacent to the two basins of attraction. Since these dihedral angles are defined by the centroids of six-membered rings, those benzyl rings are not necessarily in the same plane when the dihedral angles are zero. Instead, these six-membered rings can rotate out of the plane at zero or near zero dihedral angles to avoid steric clashes. This pathway, therefore, is a very efficient mechanism for the two helical structures to interconvert between each other. This deduction also agrees with the suggested mechanism (Figure 8) for the helical interconversion of **1**, as directly observed by visual analysis of the REMD trajectories (Figure 9).

A PCA was performed on the REMD simulations of **1**. This analysis generated 369 components corresponding to the total degrees of freedom for **1**. All of the components were sorted in terms of descending magnitudes by their eigenvalues (see the Supporting Information, Figure S8). The first several components contribute to the majority of the total eigenvalues, and the first 4 eigenvalues contribute more than 50% to the sum of all of the eigenvalues. Subsequent visualization of the components with the largest eigenvalues by the Visual Molecular Dynamics (VMD)[64] program with the external plug-in Interactive Essential Dynamics (IED)[65] revealed that modes 1 and 3 are directly related to the interconversion between right- and left-handed helices (Figure 12). For PCA mode 1, two azobenzene rings, depicted with two arrows pointing from right to left in Figure 12, carry the majority of the motion of this mode. Following the motions labeled by the arrows, the right part of the structure switches positions with the left part. As a result, the right-handed helix in the figure will change to a left-handed helix. In PCA mode 3, the pattern of molecular movement is similar to mode 1, but the directions of major movements are perpendicular to those in state 1. By following the motion in mode 3, the conformation of the molecule can change between the two helical structures.
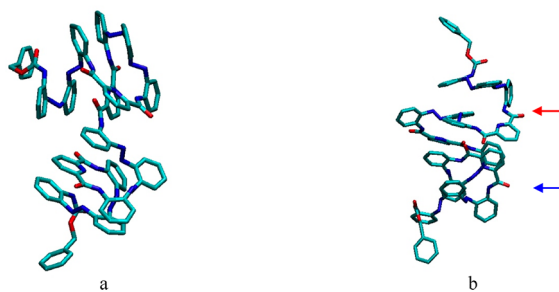
Figure 12. Major displacement represented by principal component analysis (PCA) modes 1 and 3 of **1**.

Combined together, these two modes describe the interconversion between the two helices.

E. REMD Simulation of 2. REMD simulations were applied to simulate the interconversion of the longer oligomer **2**. The average acceptation ratio for exchange is 0.472 in REMD simulation of **2**. The acceptation ratio for each individual replica is listed in Table S2 in the Supporting Information.

The starting geometry of the REMD simulation had half of the structure being a left-handed and the other half being a right-handed helix (Figure 6). A conformer with both segments in a right-handed helical conformation was found among the REMD trajectories (Figure 13a). The existence of this

Figure 13. Starting with the mixed (half right-handed and half left-handed helical) structure from Figure 6, conformers of **2** obtained from the REMD simulations are shown. (a) This conformer has both halves of the molecule in a right-handed helical conformation. (b) This conformer has both unfolded and extended structures as depicted by the red and blue arrows, respectively.
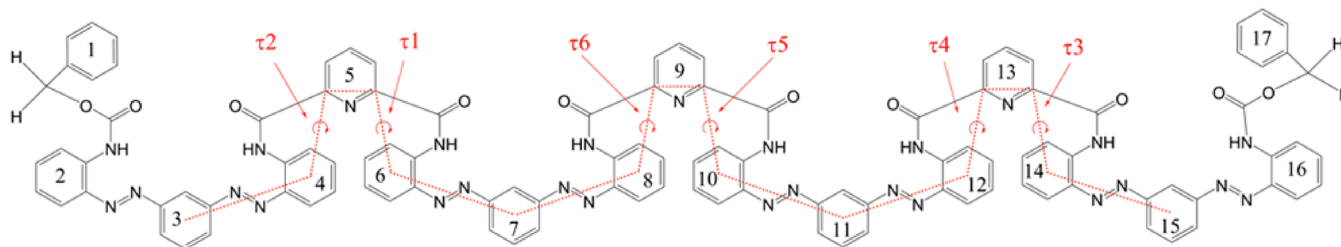
conformer indicates that conversion from a left to a right-handed helix occurred during the REMD simulations. The conformer with an unfolded helix was also discovered from the

REMD trajectories of **2** (Figure 13b). The unfolded part in Figure 13b is involved with rotation of the two six membered (pyridine and phenyl) rings. This is similar to the intermediate structure (Figure 8) for the helical interconversion observed in the REMD simulations of **1**. Thus, a similar mechanism is operative for the helical interconversion of **2**.
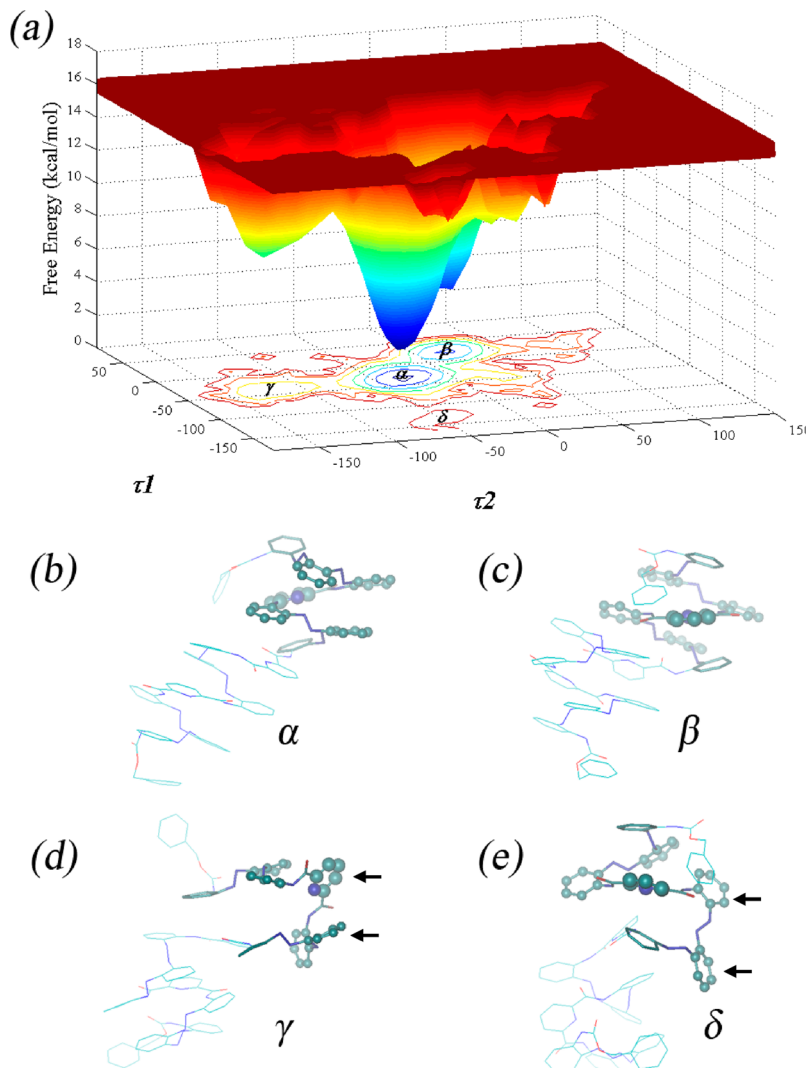
Six dihedral angles ($\tau_1 - \tau_6$) in **2** are defined in Figure 14, and were used in the T-WHAM analysis. There are three pyridine rings as linkages between the azobenzene units in **2**. The free energy contour plot at 300 K, as projected onto τ_1 and τ_2, is shown in Figure 15a. Two major attraction basins (α and β) are located on the diagonal line. This pattern is very similar to the PMF contour of dihedral angles based on the REMD simulation of **1** (Figure 11). The portion of the structure related to τ_1 and τ_2 in **2** has the same structural unit as **1**. This observation indicates that this part of the molecule in **2** can fold into either a right- or left-handed helix. The representative conformers of α and β basins are illustrated in Figure 15b and c, respectively. The portions of molecules defining τ_1 and τ_2 in **2** (this portion of molecule will be designated as upper part for convenience) are shown in ball and stick mode for clarity. Similar to the PMF of **1** (Figure 11), the lower left diagonal basin (α) corresponds to the left-handed helix for the upper part of **2**. The upper right diagonal basin (β) corresponds to the right-handed helix for the upper part of **2**.

Besides the diagonal attraction basins, there is another major off-diagonal basin (γ), and one minor off-diagonal basin (δ). Interestingly, the representative conformers of both basin γ (Figure 15d) and basin δ (Figure 15e) have the upper part of **2** in a twisted intermediate conformation of **1** (Figure 8b). In both conformers, as shown in Figure 15d and e, the rings that rotate away from the helical structure (shown with arrows) are those that define dihedral angle τ_1 (Figure 14). On the contrary, rings defining τ_2 remain as in the helical structure. The difference between τ_1 and τ_2 is that rings 6 and 7, which define τ_1, are closer to the molecular center than rings 3 and 4, which define τ_2 (Figure 14). Rings with arrows in Figure 15d and e correspond to rings 6 and 7 in Figure 14. This observation indicates that rings 6 and 7 are more likely rotated into a twisted intermediate structure than rings 3 and 4.

The PMF of the free energy at 300 K projected onto τ_3 and τ_4 are shown in Figure 16a. Similar to the PMF of τ_1 and τ_2, two major diagonal attraction basins (ϵ and ζ) are shown in this plot. The representative conformers of ϵ and ζ basins are illustrated in Figure 16b and c, respectively. The molecular portions that define τ_3 and τ_4 in **2** (we will refer to this region as the lower part for convenience) are shown in ball and stick for clarity. The lower left diagonal basin (ϵ) corresponds to the left-handed helix of the lower part of **2**. The upper right

Figure 14. Definitions of dihedral angles in **2** for subsequent T-WHAM analysis. The six dihedral angles ($\tau_1 - \tau_6$) are defined by two carbon atoms adjacent to the nitrogen in the central pyridine ring (ring 5, 9, and 13) and the centroids of two benzene rings next to pyridine on either side (ring 3, 4, 6, 7, 8, 10, 11, 12, 14, and 15).

Figure 15. The potential of mean force (PMF) contour plots at 300 K projected onto the dihedral angles τ_1 and τ_2 (see Figure 14) for the REMD simulation of **2**: (a) PMF plot; (b) representative conformer of attraction basin α (highlighted segment is a left-handed helix); (c) representative conformer of attraction basin β (highlighted segment is a right-handed helix); (d) representative conformer of attraction basin γ (highlighted segment is a twisted intermediate structure); (e) representative conformer of attraction basin δ (highlighted segment is a twisted intermediate structure). Different parts of molecule **2** are shown in different forms for clarity: Rings defining τ_1 and τ_2 are shown in ball and stick. Carboxamide and N=N linkers among those rings and two adjacent phenyl rings are shown in tube format; all of the other parts are shown in line format. Atoms are colored according to atom types (C, N, and O are shown in cyan, blue, and red, respectively). Hydrogen atoms are not shown. The same color scheme is also used in Figures 16, 17, and 18.
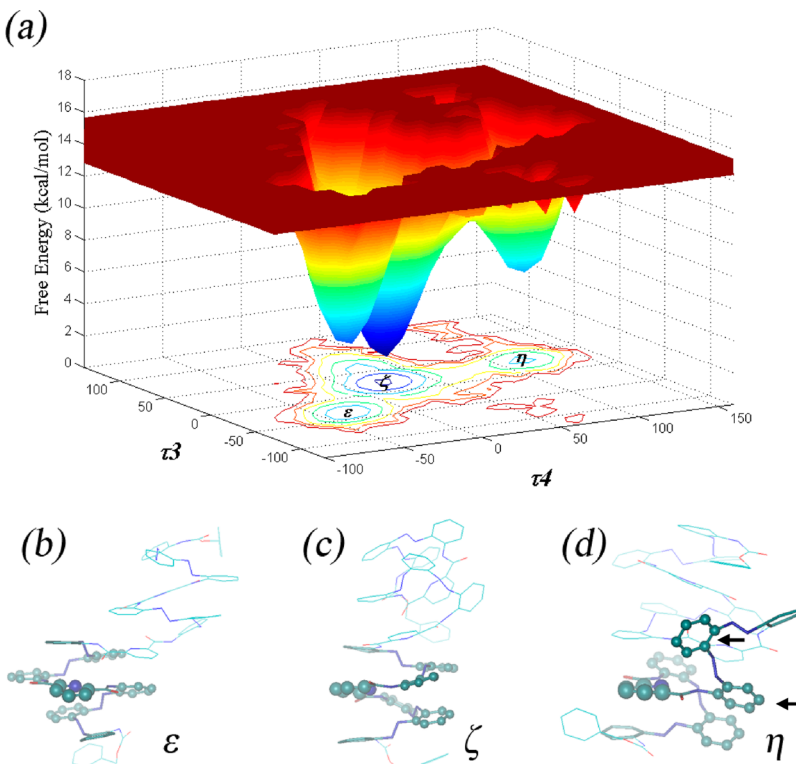
diagonal basin (ζ) corresponds to the right-handed helix of the lower part of **2**.

One major off-diagonal attraction basin (η) is shown in the plot with a representative conformer illustrated in Figure 16d. The η conformer is also a twisted intermediate with two phenyl rings rotating away from a helical structure (shown with arrows in Figure 16d). Interestingly, these two rings are rings 11 and 12 in Figure 14, and define the dihedral angle τ_4. Rings 14 and 15 remain as in the helical structure in this conformer. This indicates that rings 11 and 12 are more likely rotated into twisted intermediate structures than rings 14 and 15.

It is a very interesting coincidence that, in both upper and lower part of **2**, rings that are close to the molecular center (Figure 14: 6−7 and 11−12 pairs) are more likely to rotate away from a helical structure into a twisted intermediate than rings that are close to the molecular termini (Figure 14: 3−4 and 14−15 pairs). This counterintuitive observation provides

an important hint for the helical interconversion process, in which the interconversion is more likely to start from the central part of the molecule instead of the two termini.

The PMF plot of **2** with respect to τ_5 and τ_6 is plotted in Figure 17a. The PMF contour plot is significantly different from the earlier ones for τ_1 through τ_4. In Figure 17a, there is no diagonal attraction basin. Two major attraction basins (θ and λ) correspond to τ_5 near 0° and τ_6 in the ranges from −150° to −100° and 50° to 100°. The representative conformers of the θ and λ basins are illustrated in Figure 17b and c, respectively. The portion of the molecule that defines τ_5 and τ_6 in **2** (we will refer to this region as the central region for convenience) is shown in ball and stick mode for clarity. This central region contains the parts of **2** from ring 7 to 11 (Figure 14). As shown in Figure 17b and c, the central region does not adopt a helical structure at either attraction basin. The pyridine ring in the central region (ring 9 in Figure 14) divides **2** into two parts
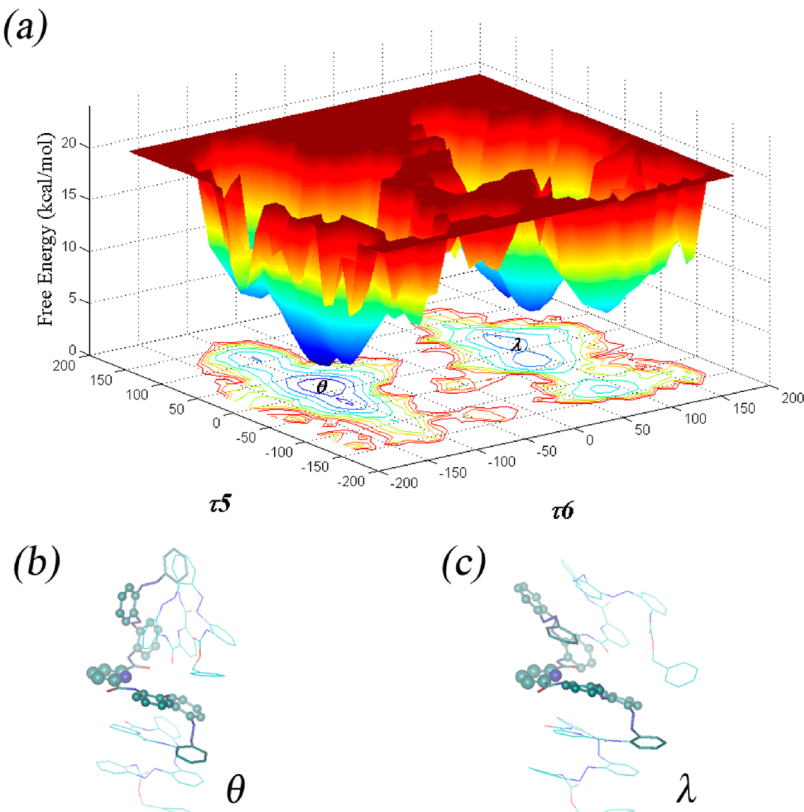
Figure 16. Potential of mean force (PMF) contour plots at 300 K projected onto the dihedral angles τ_3 and τ_4 (see Figure 14) for the REMD simulation of **2**: (a) PMF plot; (b) representative conformer of attraction basin ε (highlighted segment is a left-handed helix); (c) representative conformer of attraction basin ζ (highlighted segment is a right-handed helix); (d) representative conformer of attraction basin η (highlighted segment is a twisted intermediate structure). Different parts of molecule are shown in different form for clarity: Rings defining τ_3 and τ_4 are shown in ball and stick. Carboxamide and N=N linkers among those rings and two adjacent phenyl rings are shown in tube format; the rest of the molecule is shown in line format.

(upper and lower, as discussed above). These two parts do not correlate to each other strongly and can adopt helical structures independently. In addition, the interconversion between different helices in these two parts is not strongly correlated either. Both upper and lower parts of **2** are approximately of the same size as **1**. The behavior of **2** suggests that oligomer **1** is the approximate unit size for helical structure formation and interconversion. It is also suggestive that the interconversion between different helical structures is more likely to start from the middle of the oligomer rather than from the ends. Since the upper and lower parts of **2** are structural units for helical conformations, the central region, which connects these two units, behaves more like a linker than a helical structure unit. Several typical conformers of **2** (see the Supporting Information, Figure S9) show the mutual independence between the two halves of **2**. However, because of the limited size of **2**, it is not conclusive that the center unit defined by angles θ and λ could not behave as a structural unit, or fold into a uniform helical structure. The observation of **2** only indicates that having two halves independently fold into helical structures is energetically more favorable than having central structural unit fold into helical structure. It is likely that arbitrary segments within long strand of helical structure could somewhat independently fold into either M or P helical structure. To investigate this issue, simulation and analysis of larger oligomers than **2** are necessary in future study.
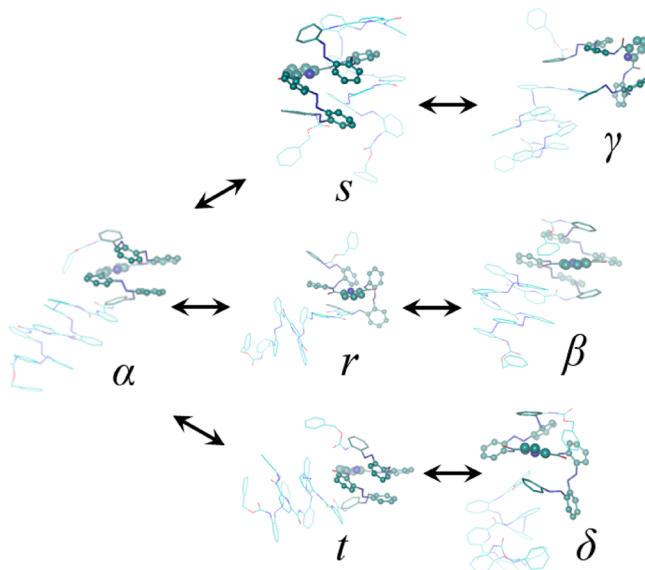
No single pair of dihedral angles alone can fully describe the interconversion process of **2**. Thus, no single interconversion barrier can be obtained from the PMF analysis of **2**. However,

the barriers for local conformational changes of **2** can be estimated and compared to experimental values. On the PMF projected onto τ_1 and τ_2 (Figure 15a), the system needs to overcome three barriers to reach the attraction basin. Interestingly, The barrier between two major basins (α and β) is around 7 kcal/mol. This is much lower than the barriers between basins α and γ and basins α and δ, which are 11 and 14 kcal/mol, respectively. In fact, the latter two barriers are comparable to the experimental value of 13.8 kcal/mol, as determined by variable temperature NMR.[25] On the PMF projected onto τ_3 and τ_4 (Figure 16a), the barrier between two major basins (ε and ζ) is 9 kcal/mol and is lower than the barrier between basins ζ and η (11 kcal/mol). The PMF projected onto τ_5 and τ_6 (Figure 17a) has two large major attraction basins (θ and λ) with barrier around 16 kcal/mol between them. As summary, the highest barriers for system to reach each attraction basins on three PMF surfaces discussed are 14, 11, and 16 kcal/mol, respectively. All the differences between these numbers and experimental values are less than 3 kcal/mol.

Several conformers were selected to represent the intermediates among attraction basins on PMF projected onto τ_1 and τ_2 (Figure 18). Since basin α directly connects with other three basins (Figure 15a), the selected intermediate conformers represent the pathways of local conformational changes from basin α to other basins on the surface. Conformer r connects basins α and β. The structure of this half of the molecule in r is quite similar to the intermediate conformer for the helical interconversion of **1** (Figures 8 and 9). This

Figure 17. The potential of mean force (PMF) contour plots at 300 K projected onto the dihedral angles τ_5 and τ_6 (see Figure 14) for the REMD simulation of **2**: (a) PMF plot; (b) representative conformer of attraction basin θ; (c) representative conformer of attraction basin η. Different parts of molecule **2** are shown in different forms for clarity. Rings defining τ_5 and τ_6 are shown in ball and stick. Carboxamide and N=N linkers among those rings and two adjacent phenyl rings are shown in tube format; the rest is shown in line format.

Figure 18. Representative conformers that connect basin α to basins β, γ, and δ on τ_1 and τ_2 PMF (Figure 15a). Conformer r connects two major basins (α and β), and the structure of the highlighted half is similar to the intermediate conformer for the helical interconversion of **1** (Figures 8 and 9). Conformers s and t connect basin α to γ and δ, respectively, through local conformational changes.

observation strongly supports that the helical structure interconversion of these oligomers are localized through a uniformed mechanism. The other two intermediate conformers

s and t are also involved local changes to connect basin α to two minor basins (γ and δ).

Thus, the REMD simulations of **1** and **2** reveal that the dynamic unit of these oligomers is roughly the size of **1**, or one-half of **2**. This structural unit can independently convey information about the helical fold. Essentially, the two structural subunits in **2** can fold into different helices, and do not show strong coupling with each other. The interconversion mechanism observed in the REMD simulation of **1**, therefore, was also applicable to either the upper or the lower subunit of **2**.

F. NEB Reaction Path for Helical Interconversion of 2. To demonstrate the independence between two structural units in **2**, the NEB calculations were carried out to search an interconversion pathway for only one unit. The geometries shown in Figure 15 were used to construct the initial path. A total of 16 replicas were built for the NEB path by making multiple copies for initial geometries. The final path demonstrates that the interconversion between two helices for one structural unit has no significant effect on the other unit (Figure S10 in the Supporting Information). The helical interconversion of the target unit is achieved through the local movement similar to those shown in the NEB path of **1**, while the other unit remains essentially intact throughout the transition.

IV. CONCLUSIONS

This study has focused on the interconversion between the right- and left-handed helices of alternating pyridinedicarbox-amide/*m*-(phenylazo)azobenzene oligomers. The systematic

torsional sampling Monte Carlo method was used to sample both right- and left-handed helices of **1**. Most of the MC-generated conformers with high energies have extended structures, and the low-energy conformers have helical structures. However, due to the correlated motion of these units, information about the mechanism of interconversion between helical conformations cannot be obtained from MC sampling approach. The MC multiple minimum (MCMM) search algorithm was employed for the conformational search of **2**. The interconversion between helices was not observed in the MC simulations of **2** either.

Replica-exchange molecular dynamics (REMD) was applied to simulate the interconversion process for oligomers **1** and **2**. Indeed, interconversion between the two helices was observed in both REMD trajectories and has calculated barriers for interconversion that are very similar to the experimental values. The right-handed helix of **1** changed to a left-handed helix through a mechanism involving the rotations of the central pyridinedicarboxamide ring and one adjacent benzyl ring. The rotational motion of these two aromatic rings leads to unwinding of the helical structure and eventually conversion of the helix from one handedness to the other. This conversion is relatively local and does not go through a fully extended structure of **1**. The intermediate structures along the conversion path are rather compact (Figures 8 and 9). The localized conversion mechanism is supported by several studies that showed that the barriers of interconversion between M and P helical structures are independent of the size of helical structures.[22,24,25]

Conversion of a helix was also observed in the simulations of **2**. The interconversion between two helices of **2** is also involved with the rotation of two pyridinedicarboxamide moieties, which is similar to the conversion mechanism observed for **1**. The potential of mean force analysis of **2** indicates that the interconversion between two helices is more likely to start from the central part of the helix than a segment closer to a terminus of the oligomer. REMD simulations of **1** and **2** indicate that the relatively independent structural unit for folding and structural interconversion is roughly the size of oligomer **1**. The structural unit of this size can convert to a different helix without necessary coupling to adjacent structural moieties. This observation is in good agreement with the observation of M and P segments packing in helical polymers in a two-dimensional (2D) crystal state[23] and indicates that the helical structures with different handedness interconvert through a compact and partially folded structure instead of a globally unfold and extended structure. This finding provides insight into the structural and dynamical properties of non-natural oligomers and could aid in the design of new oligomers with helical structures. Moreover, the T-WHAM and PMF analyses, as utilized here, may be of great value in the analysis of interconversion processes for larger folding oligomers.

ASSOCIATED CONTENT

Ⓢ Supporting Information

^{1}H NMR chemical shift of **1**, exchange acceptation ratio of REMD for **1** and **2**, rmsd and dihedral angle distribution of 100 ns MD simulation of **1** and **2**, representative conformers of **2** from MD, MC and REMD simulations, superimpose of selective REMD structures and crystal structures of **1**, NEB helical interconversion paths for **1** and **2**, PCA analysis of **1**, movie clip of part of REMD trajectory of **1** showing conformation change from twisted intermediate structure to left-handed helix. This material is available free of charge via the Internet at http://pubs.acs.org.

AUTHOR INFORMATION

Corresponding Author
*Fax: (614) 292-1685. E-mail: hadad.1@osu.edu.

Present Address
†Laboratory of Computational Biology, National Heart, Lung and Blood Institute, National Institutes of Health, Bethesda, Maryland, 20852

Notes
The authors declare no competing financial interest.

REFERENCES

(1) Nakano, T.; Okamoto, Y. *Chem. Rev.* **2001**, *101*, 4013−4038.
(2) Sanford, A. R.; Gong, B. *Curr. Org. Chem.* **2003**, *7*, 1649−1659.
(3) Cheng, R. P. *Curr. Opin. Struct. Biol.* **2004**, *14*, 512−520.
(4) Licini, G.; Prins, L. J.; Scrimin, P. *Eur. J. Org. Chem.* **2005**, 969−977.
(5) Kanamori, D.; Okamura, T.-A.; Yamamoto, H.; Ueyama, N. *Angew. Chem., Int. Ed.* **2005**, *44*, 969−972.
(6) Stone, M. T.; Moore, J. S. *J. Am. Chem. Soc.* **2005**, *127*, 5928−5935.
(7) Nelson, J. C.; Saven, J. G.; Moore, J. S.; Wolynes, P. G. *Science* **1997**, *277*, 1793−1796.
(8) Hofacker, A. L.; Parquette, J. R. *Angew. Chem., Int. Ed.* **2005**, *44*, 1053−1057.
(9) Goto, K.; Moore, J. S. *Org. Lett.* **2005**, *7*, 1683−1686.
(10) Chang, K.-J.; Kang, B.-N.; Lee, M.-H.; Jeong, K.-S. *J. Am. Chem. Soc.* **2005**, *127*, 12214−12215.
(11) Petitjean, A.; Nierengarten, H.; van Dorsselaer, A.; Lehn, J.-M. *Angew. Chem., Int. Ed.* **2004**, *43*, 3695−3699.
(12) Gellman, S. H. *Acc. Chem. Res.* **1998**, *31*, 173−180.
(13) Cubberley, M. S.; Iverson, B. L. *Curr. Opin. Chem. Biol.* **2001**, *5*, 650−653.
(14) Hill, D. J.; Mio, M. J.; Prince, R. B.; Hughes, T. S.; Moore, J. S. *Chem. Rev.* **2001**, *101*, 3893−4011.
(15) Morino, K.; Maeda, K.; Yashima, E. *Macromolecules* **2003**, *36*, 1480−1486.
(16) Hill, D. J.; Moore, J. S. *Proc. Natl. Acad. Sci. U.S.A.* **2002**, *99*, 5053−5057.
(17) Nakashima, H.; Fujiki, M; Koe, J. R.; Motonaga, M. *J. Am. Chem. Soc.* **2001**, *123*, 1963−1969.
(18) Nakako, H.; Nomura, R.; Masuda, T. *Macromolecules* **2001**, *34*, 1496−1502.
(19) Fujiki, M. *J. Am. Chem. Soc.* **2000**, *122*, 3336−3343.
(20) Boiadjiev, S. E.; Lightner, D. A. *J. Am. Chem. Soc.* **2000**, *122*, 378−383.
(21) Lifson, S.; Felder, C. E.; Green, M. M. *Macromolecules* **1992**, *25*, 4142−4148.
(22) Ohkita, M.; Lehn, J.; Baum, G.; Fenske, D. *Chem.—Eur. J.* **1999**, *5*, 3471−3481.
(23) Sakurai, S.; Ohsawa, S.; Nagai, K.; Okoshi, K.; Kumaki, J.; Yashima, E. *Angew. Chem., Int. Ed.* **2007**, *46*, 7605−7608.
(24) Delsuc, N.; Kawanami, T.; Lefeuvre, J.; Shundo, A.; Ihara, H.; Takafuji, M.; Huc, I. *ChemPhysChem* **2008**, *9*, 1882−1890.
(25) Tie, C; Gallucci, J. C.; Parquette, J. R. *J. Am. Chem. Soc.* **2006**, *128*, 1162−1171.

(26) King, E. D.; Tao, P.; Sanan, T. T.; Hadad, C. M.; Parquette, J. R. *Org. Lett.* **2008**, *10*, 1671–1674.

(27) Brooks, B.; Karplus, M. *Proc. Natl. Acad. Sci. U.S.A.* **1983**, *80*, 6571–6575.

(28) Wynsberghe, A.; Van; Cui, Q. *Structure* **2006**, *14*, 1647–1653.

(29) Liu, J; Nussinov, R. *Proc. Natl. Acad. Sci. U.S.A.* **2008**, *105*, 901–906.

(30) Goodman, J. M.; Still, W. C. *J. Comput. Chem.* **1991**, *12*, 1110–1117.

(31) Fariborz Mohamadi, F.; Richards, N. G. J.; Guida, W. C.; Liskamp, R.; Lipton, M.; Caufield, C.; Chang, G.; Hendrickson, T.; Still, W. C. *J. Comput. Chem.* **1990**, *11*, 440–467.

(32) Still, W. C.; Tempczyk, A.; Hawley, R. C.; Hendrickson, T. *J. Am. Chem. Soc.* **1990**, *112*, 6127–6129.

(33) Chang, G.; Guida, W.; Still, W. C. *J. Am. Chem. Soc.* **1989**, *111*, 4379–4386.

(34) Saunders, M.; Houk, K. N.; Wu, Y.-D.; Still, W. C.; Lipton, M.; Chang, G.; Guida, W. C. *J. Am. Chem. Soc.* **1990**, *112*, 1419–1427.

(35) Cancès, E.; Mennucci, B.; Tomasi, J. *J. Chem. Phys.* **1997**, *107*, 3032–3041.

(36) Chai, J.; Head-Gordon, M. *Phys. Chem. Chem. Phys.* **2008**, *10*, 6615–6620.

(37) Zhao, Y.; Truhlar, D. G. *Theor. Chem. Acc.* **2008**, *120*, 215–241.

(38) Revilla-López, G.; Laurent, A. D.; Perpète, E. A.; Jacquemin, D.; Torras, J.; Assfeld, X.; Alemán, C. *J. Phys. Chem. B* **2011**, *115*, 1232–1242.

(39) Wolinski, K.; Hinton, J. F.; Pulay, P. *J. Am. Chem. Soc.* **1990**, *112*, 8251–8260.

(40) Frisch, M. J.; Trucks, G. W.; Schlegel, H. B.; Scuseria, G. E.; Robb, M. A.; Cheeseman, J. R.; Scalmani, G.; Barone, V.; Mennucci, B.; Petersson, G. A.; Nakatsuji, H.; Caricato, M.; Li, X.; Hratchian, H. P.; Izmaylov, A. F.; Bloino, J.; Zheng, G.; Sonnenberg, J. L.; Hada, M.; Ehara, M.; Toyota, K.; Fukuda, R.; Hasegawa, J.; Ishida, M.; Nakajima, T.; Honda, Y.; Kitao, O.; Nakai, H.; Vreven, T.; Montgomery, Jr., J. A.; Peralta, J. E.; Ogliaro, F.; Bearpark, M.; Heyd, J. J.; Brothers, E.; Kudin, K. N.; Staroverov, V. N.; Kobayashi, R.; Normand, J.; Raghavachari, K.; Rendell, A.; Burant, J. C.; Iyengar, S. S.; Tomasi, J.; Cossi, M.; Rega, N.; Millam, N. J.; Klene, M.; Knox, J. E.; Cross, J. B.; Bakken, V.; Adamo, C.; Jaramillo, J.; Gomperts, R.; Stratmann, R. E.; Yazyev, O.; Austin, A. J.; Cammi, R.; Pomelli, C.; Ochterski, J. W.; Martin, R. L.; Morokuma, K.; Zakrzewski, V. G.; Voth, G. A.; Salvador, P.; Dannenberg, J. J.; Dapprich, S.; Daniels, A. D.; Farkas, Ö.; Foresman, J. B.; Ortiz, J. V.; Cioslowski, J.; Fox, D. J. *Gaussian 09*, Revision A.1; Gaussian, Inc.: Wallingford, CT, 2009.

(41) Case, D. A.; Darden, T. A.; Cheatham, T. E.III, ; Simmerling, C. L.; Wang, J.; Duke, R. E.; Luo, R.; Merz, K. M.; Wang, B.; Pearlman, D. A.; Crowley, M.; Brozell, S. R.; Tsui, V.; Gohlke, H.; Mongan, J.; Hornak, V.; Cui, G.; Beroza, P.; Schafmeister, C.; Caldwell, J. W.; Ross, W. S.; Kollman, P. A. *AMBER*, Version 8; University of California: San Francisco, 2004.

(42) Wang, J.; Wolf, R. M.; Caldwell, J. W.; Kollman, P. A.; Case, D. A. *J. Comput. Chem.* **2004**, *25*, 1157–1174.

(43) Hawkins, G. D.; Cramer, C. J.; Truhlar, D. G. *Chem. Phys. Lett.* **1995**, *246*, 122–129.

(44) Hawkins, G. D.; Cramer, C. J.; Truhlar, D. G. *J. Phys. Chem.* **1996**, *100*, 19824–19839.

(45) Ryckaert, J. P.; Ciccotti, G.; Berendsen, H. J. C. *J. Comput. Phys.* **1977**, *23*, 327–341.

(46) Cheng, X.; Cui, G.; Viktor Hornak, V.; Simmerling, C. *J. Phys. Chem. B* **2005**, *109*, 8220–8230.

(47) Jónsson, H.; Mills, G.; Jacobsen, K. W. Nudged Elastic Band Method for Finding Minimum Energy Paths of Transitions. In *Classical and Quantum Dynamics in Condensed Phase Simulations*; Berne, B. J., Ciccotti, G., Coker, D. F., Eds.; World Scientific: Singapore, 1998; pp 385–404.

(48) Bergonzo, C.; Campbell, A. J.; Walker, R. C.; Simmerling, C. *Int. J. Quantum Chem.* **2009**, *109*, 3781–3790.

(49) Case, D. A.; Darden, T. A.; Cheatham, T. E., III; Simmerling, C. L.; Wang, J.; Duke, R. E.; Luo, R.; Walker, R. C.; Zhang, W.; Merz, K. M.; Roberts, B.; Hayik, S.; Roitberg, A.; Seabra, G.; Swails, J.; Götz, A. W.; Kolossváry, I; Wong, K. F.; Paesani, F.; Vanicek, J.; Wolf, R. M.; Liu, J.; Wu, X.; Brozell, S. R.; Steinbrecker, T.; Gohlke, H.; Cai, Q.; Ye, X.; Wang, J.; Hsieh, M.-J.; Cui, G.; Roe, D. R.; Mathews, D. H.; Seetin, M. G.; Salomon-Ferrer, R.; Sagui, C.; Babin, V.; Luchko, T.; Gusarov, S.; Kovalenko, A.; Kollman, P. A. *AMBER*, Version 12; University of California: San Francisco, 2012.

(50) Gallicchio, E.; Andrec, M.; Felts, A. K.; Levy, R. M. *J. Phys. Chem. B* **2005**, *109*, 6722–6731.

(51) Zhang, J.; Qin, M.; Wang, W. *Proteins* **2006**, *62*, 672–685.

(52) Shea, J.-E.; Nochomovitz, Y. D.; Guo, Z.; Brooks, C. L., III *J. Chem. Phys.* **1998**, *109*, 2895–2903.

(53) Ichiye, T.; Karplus, M. *Proteins* **1991**, *11*, 205–217.

(54) García, A. E. *Phys. Rev. Lett.* **1992**, *68*, 2696–2699.

(55) Amadei, A.; Linssen, A. B. M.; Berendsen, H. J. C. *Proteins* **1993**, *17*, 412–425.

(56) Hayward, S.; Kitao, A.; Hirata, F.; Go, N. *J. Mol. Biol.* **1993**, *234*, 1207–1217.

(57) Becker, O. M. *Proteins* **1997**, *27*, 213–226.

(58) de Groot, B. L.; Daura, X.; Mark, A. E.; Grubmüller, H. *J. Mol. Biol.* **2001**, *309*, 299–313.

(59) Tournier, A. L.; Smith, J. C. *Phys. Rev. Lett.* **2003**, *91*, 208106/1–208106/4.

(60) Nguyen, P. H.; Mu, Y.; Stock, G. *Proteins* **2005**, *60*, 485–494.

(61) Nguyen, P. H.; Stock, G.; Mittag, E.; Hu, C.-K.; Li, M. S. *Proteins* **2005**, *61*, 795–808.

(62) Kitao, A.; Hirata, F.; Go, N. *Chem. Phys.* **1991**, *158*, 447–472.

(63) Gabriel, C. J.; DeMatteo, M. P.; Paul, N. M.; Takaya, T.; Gustafson, T. L.; Hadad, C. M.; Parquette, J. R. *J. Org. Chem.* **2006**, *71*, 9035–9044.

(64) Humphrey, W.; Dalke, A.; Schulten, K. *J. Mol. Graph.* **1996**, *14*, 33–38.

(65) Mongan, J. *J. Comput.-Aided Mol. Des.* **2004**, *18*, 433–436.